THE JOURNAL OF PHYSICAL CHEMISTRY C

Article

pubs.acs.org/JPCC

A Comparative First-Principles Study on Sodiation of Silicon, Germanium, and Tin for Sodium-Ion Batteries

Chia-Yun Chou,[†] Myungsuk Lee,[‡] and Gyeong S. Hwang*[,†,‡]

[†]Materials Science and Engineering Program and [‡]McKetta Department of Chemical Engineering, University of Texas at Austin, Austin, Texas 78712, United States

Supporting Information

ABSTRACT: Sodium-ion batteries (NIBs) have recently received great attention as a potential complement to existing lithium-ion battery (LIB) technology. Because of the difference between Na and Li in nature, what has been an attractive anode material for LIBs may or may not be utilized for NIBs. Using density functional theory calculations, we examine and compare the sodiation behaviors of Si, Ge, and Sn, in comparison also to their lithiation processes if needed. We evaluate single Na incorporation in the host matrices (M = Si, Ge, Sn) and also discuss the formation of Na−M alloys in terms of structural evolution and energetics, along with their mechanical and diffusion properties. While the alloy systems considered in this work appear to undergo similar transformation during sodiation and lithiation, the M networks tend to lose connectivity more rapidly in the former. At Na/Li:M = 1:1 ratio, the M networks in *a*-NaM alloys already disintegrate into compact isolated clusters while those in *a*-LiM still maintain extended connectivity via puckered conformation. This unique difference in their specific atomic arrangements contributes to the more rapid softening, larger volume expansion, and faster increase in Na diffusivity with sodiation in comparison to the case of lithiation.

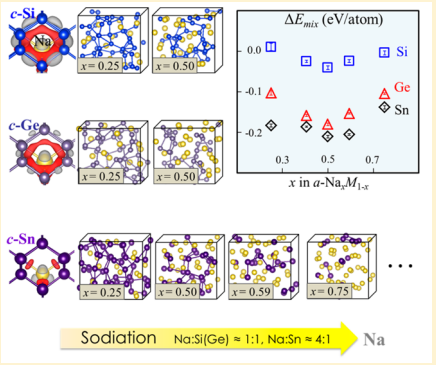

1. INTRODUCTION

Lithium-ion batteries (LIBs)[1,2] currently dominate the electrical energy storage market for portable applications; their appealing attributes may include that Li is the lightest metallic element with a small ionic radius and has very low redox potential, which enables cells with high energy density, rate capability, and voltage. However, with the enormous demand for LIBs as a major power source in electronics and vehicles, the availability of Li resources and rising price become a daunting concern, which leads to the search for different energy storage systems in parallel. Among the possible alternatives, sodium (Na), located right below Li in the periodic table, has an electrochemical Na/Na^+ redox potential only 0.3 V above that of Li/Li^+.[3] While the fundamental principles of NIBs and LIBs are identical, Na is widely abundant and costs much less than Li,[4−6] which offers great advantages targeting large-scale and stationary storage applications.

While NIBs are gaining momentum in energy storage research, most exploration has been focused on the development of cathode materials, for which metal oxides and other polyanion compounds used in LIBs also seem to work for NIBs.[7] The corresponding anode materials, on the other hand, are much less studied, and an in-depth understanding of the sodiation mechanisms and chemistries is largely lacking. Furthermore, unlike the case of LIB, graphite cannot be readily used as the anode material for NIB because Na atoms are kinetically too sluggish to intercalate into graphite basal planes (~NaC_{186}),[8] which in turn causes severe Na electroplating and detrimental dendrite formation.[9,10] Therefore, assuming the development of a cathode electrode is moving ahead, the next imminent challenging is finding a comparable anode material for NIBs to be commercially viable.

Thus far, few materials involving different sodiation mechanisms (intercalation, conversion, and alloying mechanisms)[7] have been considered for NIB anodes. Among them, alloy-type materials have received increasing attention due to their large sodiation capacities, such as NaSi (954 mAh g^{-1}),[9] NaGe (369 mAh g^{-1}),[9] $Na_{15}Sn_4$ (847 mAh g^{-1}),[9] $Na_{15}Pb_4$ (485 mAh g^{-1}),[9] and Na_3Sb (660 mAh g^{-1}).[11,12] However, their utilization is still challenging due to the significant volume expansion, which leads to anode degradation and poor capacity retention during cycling.[9,13,14]

Experimentally, group IV elements (Si, Ge, and Sn) have been well studied as anode materials for LIBs,[15−19] but the evaluation of their application in NIBs has just begun both experimentally and theoretically.[3,7,9,20] Previously, quantum-mechanical calculations based on density functional theory (DFT) have been successfully employed to develop a comprehensive understanding of the lithiation properties of Si, Ge, and Sn;[21−24] similar approaches can be extended to assess their sodiation properties in order to speed up the discovery and development of anode materials for NIBs.

Received: February 2, 2015
Revised: June 8, 2015
Published: June 12, 2015

DOI: 10.1021/acs.jpcc.5b01099
J. Phys. Chem. C 2015, 119, 14843−14850

In this work, we use DFT calculations to examine and compare the sodiation behaviors of Si, Ge, and Sn. We first investigate the atomic structure, stability, and bonding mechanisms of interstitial Na in crystalline Si, Ge, and Sn and how Na migration is influenced by its bonding interaction with the host matrix. Only the diamond structure is considered for crystalline host matrices (= Si, Ge, Sn) for direct comparison, although other allotropes (β-Ge and β-Sn)[25] may exist. Then, DFT-based *ab initio* molecular dynamics (AIMD) simulations are performed to determine the atomic configurations of amorphous Na−M (*a*-Na−M) alloys (ranging from low to highly sodiated phases). For each alloy system, we analyze the structural evolution with Na content and evaluate its relative stability in connection to the sodiation capacity by calculating mixing/formation enthalpies. We also examine the variations in Na diffusivity and bulk modulus to assess the relationship between the atomic structure and the diffusion and mechanical properties, as the alloy structure undergoes considerable changes. Comparisons between the lithiation and sodiation properties of Si, Ge, and Sn are also made whenever the opportunity presents itself. The fundamental findings may help improve the understanding of the sodiation processes in group IV materials and further explain the differences in their applications to NIBs and LIBs.

2. COMPUTATIONAL METHODS

Our DFT calculations within the Perdew−Wang 91 generalized gradient approximation (GGA-PW91)[26] were performed using the Vienna Ab-initio Simulation Package (VASP).[27−29] We used the projected augmented wave (PAW) method to describe the interaction between ion core and valence electrons and a plane-wave basis set with a kinetic energy cutoff of 350 eV (except for in mechanical property calculations where an increased cutoff energy of 450 eV was employed). The crystalline host matrices considered (*c*-M = Si, Ge, Sn) were modeled using 64-atom cubic supercells. The atomic configurations and energetics reported herein were calculated by relaxing all constituent atoms using the conjugate gradient method until the residual forces on each atom became smaller than 5×10^{-2} eV/Å; in mechanical property calculations, the convergence criteria was tightened up to 1×10^{-6} eV. We performed the Brillouin zone integration for periodic 64-atom supercells using a $(4 \times 4 \times 4)$ Monkhorst−Pack[30] mesh of *k*-points; the *k*-point mesh sizes used for crystalline alloys of various compositions and supercell sizes are specified in the text otherwise. We determined diffusion pathways and barriers using the climbing-image nudged elastic band method;[31] for each hopping step, typically eight intermediate images were employed.

We obtained the model structures for amorphous *a*-Na−M using Ab-initio Molecular Dynamics (AIMD) simulations on the basis of the atomic configurations of *a*-Li−M alloys from previous studies (see ref 32 for computational details); as reasoned below, this approach turned out to be appropriate for creating optimal *a*-Na−M structures (at a significantly reduced computational burden when compared to starting with crystalline initial configurations). The local atomic configurations (or short-range order) of the Na−M and Li−M alloys tend to be dissimilar, as the Na−M interactions differ from the Li−M interactions in nature. Nonetheless, the *a*-Li−M structures are likely good initial configurations for generating the *a*-Na−M structures (in which Na atoms are also well dispersed in M); moreover, Na and M atoms are highly mobile at elevated temperatures, allowing facile local structure rearrangements to yield optimal *a*-Na−M configurations within a moderate annealing time. After replacing Li (in *a*-Li−M alloys) with Na, we annealed the *a*-Na−M structures, each containing 64 Na and M atoms, at 1500 K for 2 ps and then rapidly quenched to 300 K at a rate of 0.6 K/fs; here, a time step of 1 fs was used, and the volume of each simulation cell was allowed to vary. We used a velocity rescaling method to control the temperature and set the annealing temperature far above the alloy melting point (~1200 K) in order to speed up the melting process while eliminating any memory effects from the initial configuration.

3. RESULTS AND DISCUSSION

A. Na Atom Behavior in Si, Ge, and Sn. *A.1. Configuration and Energetics.* We first determined and compared Na insertion in a crystalline host matrix *c*-M. In all the three host materials, the tetrahedral (T) interstitial configuration has been identified to be the most favorable energetically. Upon the Na insertion, neighboring host atoms undergo strain-induced outward relaxation. To assess the relative ease of Na accommodation and corresponding host-lattice disturbances, we compared the energy (E_f) required for single Na insertion in a 64-atom *c*-M cubic supercell, displacements (Δ) of the first- and second-nearest neighbors (NN^{1st} and NN^{2nd}), and the resulting volume expansion, as presented in Table 1.

Table 1. Predicted Formation Energies (E_f in eV) for Na at the Tetrahedral Interstitial Site in Crystalline Host Matrices (= Si, Ge, and Sn) from 64-Atom Supercell Calculations with Calculated Lattice Constants (*a*), First- and Second-Nearest-Neighbor Displacements in Å (Δ, NN^{1st}/NN^{2nd}), and the Corresponding Volume Expansions (ΔV)

	a (Å)	E_f^a (= E_s + E_e)	Δ, NN^{1st}/ NN^{2nd}	ΔV (%)
Si	5.457	1.90 (= 0.58 + 1.32)	0.17/0.07	1.50
Ge	5.777	0.88 (= 0.48 + 0.40)	0.16/0.07	1.80
Sn	6.645	−0.09 (= 0.19 − 0.28)	0.13/0.04	0.90

[a]For each case, the E_f is decomposed into the electronic (E_e) and strain (E_s) contributions.

Overall, the degrees of displacements are found to be the largest in *c*-Si and smallest in *c*-Sn while ΔNN^{2nd} are significantly smaller than ΔNN^{1st}. These results indicate that the Na insertion-induced mechanical strain is the highest in *c*-Si, lowest in *c*-Sn, and drops quickly beyond the four NN^{1st}; this trend can be understandable considering the difference in the effective interstitial space and stiffness between the host matrices. Given that the three host lattices have the same crystal (diamond) structure, we can expect the one with a bigger atomic size to have a larger effective space for accommodation of Na interstitials, thereby yielding smaller ΔNN^{1st} (and ΔNN^{2nd}). The same effect can also be anticipated from a host matrix with higher bulk modulus as it indicates a stiffer lattice to withstand the Na incorporation. Note that the covalent radii (predicted bulk moduli) for Sn, Ge, and Si are 1.40 Å (91 GPa), 1.22 Å (57 GPa), and 1.11 Å (37 GPa), respectively. Apparently, the relatively spacious Sn undergoes a minimum degree of Na-induced lattice distortion. Comparing Si and Ge, Ge has a slightly larger interstitial space but softer; considering both the geometrical and mechanical factors, the extents of outward relaxation for these two host lattices are very

DOI: 10.1021/acs.jpcc.5b01099
J. Phys. Chem. C 2015, 119, 14843−14850

comparable. Consequently, the volume expansion associated with one Na insertion is also the smallest in Sn while slightly larger in Ge and Si.

Listed in Table 1 are the formation energies (E_f) of interstitial Na in crystalline Si, Ge, and Sn. Here, the E_f is estimated relative to *c*-M and body-centered cubic Na (*bcc*-Na), i.e., $E_f = E_{Na+M} - (E_{Na} + E_M)$, where E_{Na+M} and E_M are the total energies of 64-atom *c*-M with one Na interstitial and 64-atom *c*-M, respectively, and E_{Na} is the energy per atom of *bcc*-Na. Among the host materials considered, E_f is the highest in Si (1.90 eV), lower in Ge (0.88 eV), and the lowest in Sn (−0.09 eV); the more positive value indicates that the incorporation of Na becomes less favorable. The variation for E_f in different hosts can mainly be ascribed to two factors: (a) *lattice strain*, i.e., the strain induced by Na insertion may cause weakening of the host-atom bonding and thus the increase in energy, and (b) *electronic interaction* among the Na and host atoms (accompanied by charge transfer to the host matrix from Na) which would partially compensate for the strain effect.

In order to assess the relative strain and electronic contributions (although they are closely correlated), we calculated the energy associated with distorting a pure *c*-M host lattice to what it would be after Na insertion (referred to as E_s); the difference between E_s and E_f can be attributed to the electronic interaction among the Na and host atoms (E_e).

$$E_s = E_{M'} - E_M$$

$$E_e = E_f - E_s = E_{Na+M} - (E_{Na} + E_{M'})$$

where E_M and $E_{M'}$ represent the total energies of *c*-M before and after Na insertion, respectively.

As summarized in Table 1, we can see that the E_s values are not significantly different between the three host lattices (although E_s is smaller for Sn than Ge and Si because of the softer matrix and smaller lattice distortions). Contrarily, the variation between E_e in different hosts is substantial; E_e is negative only in Sn, indicating the affinity between Na and Sn is significantly higher than that between Na and Ge (Si). Looking at the variations of E_s and E_e, it is clear that the difference in E_f is predominantly attributed to the electronic effect, rather than the strain effect. In the next section, we will discuss the bonding interaction between Na and M in more detail.

A.2. Bonding Mechanism and Diffusion. As summarized in Table 2, our Bader charge analysis demonstrates significant

Table 2. Bader Charges Predicted for Interstitial Na and Its First- and Second-Nearest Neighbors (NN^{1st} and NN^{2nd}) in Crystalline Host Matrices (= Si, Ge, and Sn)

	Si	Ge	Sn
Na	+0.67	+0.71	+0.74
NN^{1st}	−0.20	−0.10	−0.11
NN^{2nd}	−0.11	−0.07	−0.06

electron donation from Na to the host matrices; the charge states of Na in Si, Ge, and Sn are predicted to be +0.67, +0.71, and +0.74, respectively, while the host atoms surrounding Na are negatively charged. Looking at the relative amounts of charge gains of the NN^{1st} and NN^{2nd} host atoms, it is clear that the excess charge is highly localized in Si within the NN^{1st}, leading to effectively screening (or shielding) of the Na cation, whereas the charge tends to be more delocalized in Ge and Sn. Here, it is worth pointing out that the excess electrons of the surrounding host atoms arise from electron donation from Na and other host atoms, from which charges are redistributed to screen the Na cation.

As shown in the density of states (DOS) plots for Na and its four NN^{1st} [Figure 1 (left panel)], due to the charge transfer

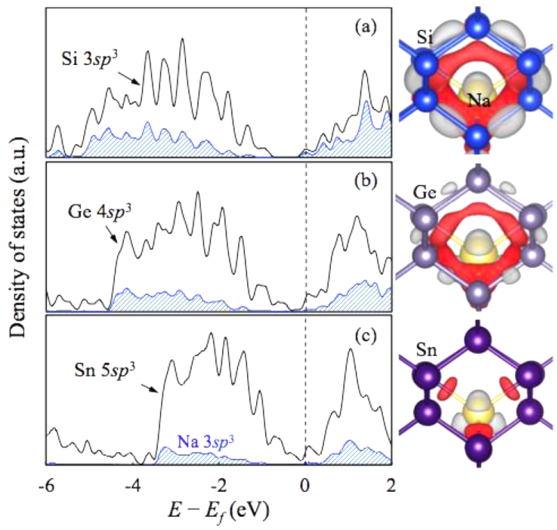

Figure 1. Left panel: projected density of states (DOS) of Na and its four nearest neighbors in crystalline Si [(a)], Ge [(b)], and Sn [(c)]. The vertical dashed line indicates the Fermi level position. Right panel: charge density differences ($\Delta\rho$) before and after Na insertion; the gray and red isosurfaces represent the regions of loss (−0.0012 e Å^{-3}) and charge gain (+0.002 e Å^{-3}), respectively.

from Na, the Fermi level is shifted above the conduction band minimum. Notice peak width for Sn $5sp^3$ < Ge $4sp^3$ < Si $3sp^3$, which is apparently due to a weaker Sn−Sn bond in comparison to Ge−Ge and Si−Si bonds; this also explains their relative bulk modulus values ($B_{Sn} < B_{Ge} < B_{Si}$). More importantly, there is substantial overlap between the Na $3sp^3$ and Si $3sp^3$ states, indicating a high degree of covalency. The Na $3sp^3$ peak intensity gradually decreases as the host matrix changes from Si to Ge to Sn. The Na−Sn hybridization appears to be relatively less strong, which is also supported by the charge density difference ($\Delta\rho$) plots in the right panel (that clearly demonstrate the lessening $\Delta\rho$ isosurface volume). The analysis implies that the Na−Sn interaction would be more ionic in nature compared to the Si and Ge cases.

Next, we evaluated the activation energies (E_a) for Na migration in the crystalline Si, Ge, and Sn matrices. As depicted in Figure 2, a Na interstitial is found to undergo migration by jumping between adjacent *T*-sites via a hexagonal (*H*)-site (saddle point). The E_a is predicted to be 1.08, 0.78, and 0.53 eV

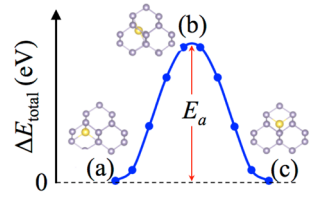

Figure 2. Predicted pathway and activation barriers (E_a in eV) for Na (Li) diffusion in crystalline Si, Ge, and Sn. Na (Li) migration occurs by jumping between two adjacent local minima located at the *T*-sites [(a) and (c)] via a hexagonal transition state at the *H*-site [(b)].

DOI: 10.1021/acs.jpcc.5b01099
J. Phys. Chem. C 2015, 119, 14843−14850

in Si, Ge, and Sn, respectively. The relatively smaller E_a in Sn can be attributed to two factors: (i) host−lattice rigidity and (ii) Na−host interaction. Among the host matrices, the more flexible lattice of Sn expands easily to allow Na to pass through, in addition to its relatively larger atomic size that renders a more effective migration channel.

In addition, a smaller E_a can also be expected if the bonding interaction between the diffusing Na and its neighboring host atoms is weaker. According to the bonding analysis discussed earlier, the degree of covalency is found to be the smallest in Na−Sn bonds, larger in Na−Ge, and the highest in Na−Si bonds. Therefore, Na can more easily migrate in M with a lower E_a. Indeed, if a Na atom was displaced from its equilibrium site (T-site) by 0.02 Å in $\pm x$, $\pm y$, and $\pm z$ directions, the restoring force experienced is predicted to be the smallest in Sn and largest in Si (see Table S1). It is also worth mentioning that, in comparison to Li diffusion in c-M,[24] the E_a values associated with Na diffusion are appreciably larger. For instance, E_a for Li diffusion in c-Si is only 0.62 eV and increases to 1.08 eV for Na diffusion. The increase in E_a would be attributed largely to the relatively larger atomic size of Na and consequently the increased covalency of Na−M bonds. Such a sizable barrier (i.e., poor rate capability) makes Si an unattractive candidate for Na-ion battery anodes; therefore, the literature focuses on Sn and occasionally Ge.

B. Structure, Energetics, and Properties of Sodiated Si, Ge, and Sn. *B.1. Energetics of Na−M Alloy Formation.* In the previous section, we examined the behavior of an isolated Na atom in group IV host matrices (c-M = Si, Ge, and Sn). From now, we discuss how the structure, energetics, and mechanical and diffusion properties of Na−M alloys vary with Na content. According to the Na−M phase diagrams, stable intermetallics can form at several Na:M composition ratios; however, room-temperature electrochemical sodiation may lead to amorphous phases. In order to evaluate the relative stabilities of Na−M alloys, we calculated the mixing enthalpies for amorphous and crystalline Na_xM_{1-x} with respect to *bcc*-Na and a-M (c-M for crystalline phases).

Figure 3 shows the predicted mixing enthalpies per atom (ΔE_{mix}); for each composition of the amorphous alloys, we obtained the average value reported based on three independent 64-atom samples. In general, all three Na−M systems shows a trend that ΔE_{mix} decreases with Na content and falls to a minimum around x = 0.5, demonstrating that the formation of Na−M alloys is energetically favorable. The deepest energy valley in the Na−Sn alloy suggests that Na−Sn alloying is the most energetically favorable, followed by Na−Ge alloying, and Na−Si alloying being the least favorable. It is also worthwhile to note that the ΔE_{mix} for the Na−Si alloy is predicted to be substantially less than that for the Li−Si alloy,[32] implying that Si sodiation may not be as facile as lithiation. Moreover, our results show that the energy valleys for the Na−Si and Na−Ge alloys occur at 50 at. % Na, while that for the Na−Sn alloy tends to shift to a higher Na content. This may suggest that Sn would have a higher sodiation capacity (per mole) than Si and Ge, which is consistent with previous experimental observations;[33,34] a fully sodiated composition for Si (Ge) is Na:Si (Ge) = 1:1 while that for Sn is found to approach Na:Sn = 3.75:1.

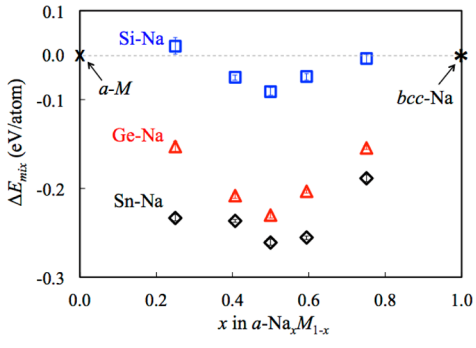

Figure 3. Variations in the mixing enthalpy per atom (ΔE_{mix}) in terms of Na content (x) for a-Na_xM_{1-x} alloys; $\Delta E_{mix} = E_{Na_xM_{1-x}} - xE_{Na} - (1 - x)E_M$, where $E_{Na_xM_{1-x}}$, E_{Na}, and E_M are the energies per atom of the alloy examined, *bcc*-Na, and a-M, respectively. Error bars are also shown but in most cases are negligible.

In addition, we calculated the formation energies (E_f) of a-Na_yM alloys as a function of Na:M ratio ($0.33 \le y \le 3$), shown in Figure 4. By neglecting the entropy and pressure terms, the free energy of the sodiated configurations (shown in Figure S1) can be approximated by the total energy at 0 K, and the E_f can be obtained by

$$E_f = E_{Na_yM} - (yE_{Na} + E_M)$$

where E_{Na_yM} is the total energy of the a-Na_yM structure divided by the number of M atoms, y is the number of Na atoms per M atom, and E_{Na} and E_M are respectively the energies per atom of *bcc*-Na and a-M.

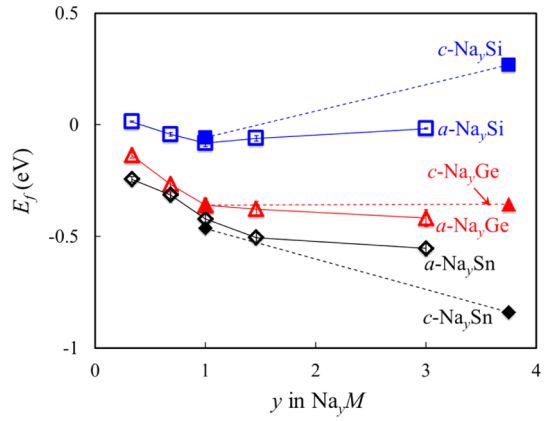

Figure 4. Formation energy (E_f) in terms of Na content (y) for a-Na_yM alloys (open symbols), estimated based on the predicted energetics in Figure 3. For comparison, the E_f of their c-Na_yM phases (y = 1 and 3.75) are also plotted (filled symbols).

The E_f of a-Na_ySn is below that of a-Na_yGe; both decrease monotonically with increasing y, but the descending trend is not as steep in a-Na_yGe alloys, especially for $y \ge 1$. Given that the negative and descending values of E_f are indicative of an energetically favorable sodiation process, our results suggest that Sn can be favorably sodiated until $y \ge 3$, while the sodiation of Ge beyond y = 1 appears to be possible but energetically less likely. (This can be clearly observed in the comparisons of the crystalline phases, although due to the amorphous nature the difference in sodiation behavior between a-Na_xGe and a-Na_xSn appears insignificant.) Conversely, the E_f of a-Na_ySi is the highest; it first exhibits a decreasing trend ($0.33 \le y \le 1$) and then increases as y becomes greater than 1, indicating that Si sodiation is only favorable up to the formation of NaSi phase.

DOI: 10.1021/acs.jpcc.5b01099
J. Phys. Chem. C 2015, 119, 14843−14850

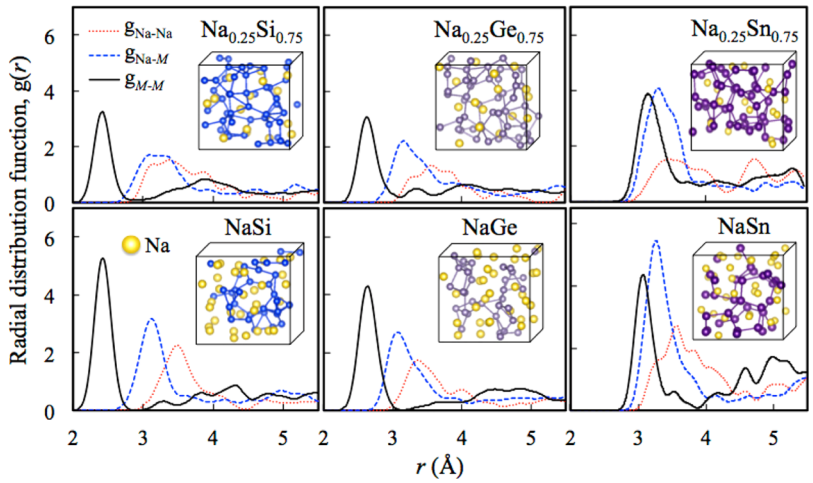

Figure 5. Radial distribution functions $g(r)$ for a-Na_xM_{1-x} alloys (x = 0.25 and 0.5) with the corresponding atomic structures shown in the inset.

Above are our assessments on the sodiation processes in Si, Ge, and Sn based on E_{mix} and E_f in the amorphous structures. Although this gives a reasonably good approximation, the values determined based on the small amorphous samples considered tend to be scattered; therefore, more accurate evaluations can be obtained based on calculations using their corresponding crystalline phases. In Figure 4, we also compare the variations in E_f for c-Na_yM as y increases from 1 to 3.75. c-$Na_{15}Si_4$ and c-$Na_{15}Ge_4$ are not stable intermetallics, but for the purpose of comparison, they were constructed to have the same crystalline structure as c-$Na_{15}Sn_4$ (see Table S2 for the corresponding crystallographic descriptions). Only in the case of Sn, the E_f of c-$Na_{3.75}M$ is lower than that of c-$Na_{1.00}M$, which clearly demonstrates that among the three host materials considered, only Sn can be favorably sodiated up to y = 3.75.

B.2. Structural Evolution and Mechanical Properties. Next, we looked at the structural evolution and mechanical properties of sodiated Si, Ge, and Sn. The structural changes of a host material M with sodiation were analyzed by calculating radial distributions functions (RDFs) for Na−Na, Na−M, and M−M pairs; the RDF plots are shown in Figure 5. Here, the RDF $g(r)$ is given by

$$g(r) = \frac{V}{N}\frac{n(r)}{4\pi r^2 \Delta r}$$

where $n(r)$ denotes particles in a shell within the region $r \pm \Delta r/2$, N is the number of particles in the model volume V, and Δr represents the shell thickness.

For the Na_xM_{1-x} alloys considered, there exhibits no sharp second-neighbor peak, confirming their amorphous-like nature (that lacks a long-range order). As the Na content increases, the Na−M and Na−Na peaks become stronger, as also seen in lithiated a-Li_xM_{1-x}.[24] However, unlike the lithiated cases, there is no significant dwindling of M−M peaks with sodiation; instead, the M−M peaks tend to become rather sharp as the Na content increases from x = 0.25 to 0.5. According to our structural analysis, this is attributed to the strong tendency of sodiated Na_xM_{1-x} alloys to form compact M clusters, leading to the sharp M−M peaks at Na:M = 1:1 ratio (see also corresponding crystalline phases in Figure S2 for clarity).

On the basis of the calculated structures, we also evaluated the changes of volume (V) with atomic ratio between Na and M (i.e., y in a-Na_yM) and compared them to those of the a-Li_yM systems as shown in Figure 6; for each alloy, the V is

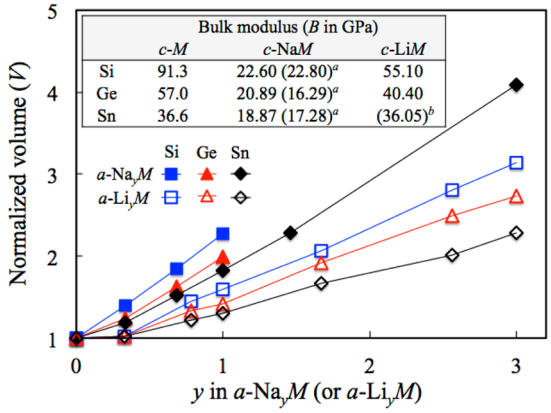

Figure 6. Variation in the volume of a-Na_yM and a-Li_yM alloys in terms of Na and Li contents (y). For each alloy, the volume (V) is normalized with respect to that of the pure a-M matrix. The calculated bulk moduli (B) of c-Na_yM and of c-Li_yM phases at y = 0 and 1 are summarized in the table (inset): a and b values are from refs 22 and 38.

normalized with respect to that of the pure amorphous host M matrix. For both sodiated and lithiated systems, V increase almost linearly with y while the former exhibits greater expansion due to the relatively larger atomic size of Na. For the a-Na_yM alloys (at y = 1), a-NaSn exhibits the least volume expansion of around 183% as compared to 227% for a-NaSi. Moreover, Sn is predicted to be further sodiated to y = 3.75 with 480% volume expansion (as estimated assuming a linear relation between V and y), which is in reasonable agreement with the experimentally observed values of 425%[35] and 520%.[36] Based on these results, it is clear that, among the three host materials considered, only Sn possess high Li and Na storage capacities with relatively low volume expansions and therefore has been the focus of investigations for both Na and Li -ion batteries.

The calculations above clearly demonstrate the structural transformation as the Na content increases. In order to evaluate how these changes affect the mechanical properties, we calculated the bulk moduli (B) of c-Na_yM phases at y = 0 and 1, which tends to be the highest sodiation concentration for Si and Ge. The B values summarized in the inset of Figure 6 are obtained by fitting the Murnaghan equation of state[37] to the corresponding energy versus volume curve; here, ±5% volume

DOI: 10.1021/acs.jpcc.5b01099
J. Phys. Chem. C 2015, 119, 14843−14850

variations in the alloys were achieved by imposing uniform tensile and compressive stresses. For comparison, we also listed the B values calculated by others (in parentheses) and the B of c-Li$_y$M (y = 0 and 1).[22,38]

$$E(V) = E_0\left(\frac{BV}{B'}\right)\left[\frac{(V_0/V)^{B'}}{B'-1} + 1\right] - \frac{V_0 B}{B'-1}$$

where E and E_0 are respectively the total energies of bulk Na$_x$M in a supercell at volume V and V_0 (equilibrium), B is the bulk modulus, and B' refers to the pressure derivative of the bulk modulus.

Our results show that the B of the c-Na$_y$M alloys decrease with Na concentration. As y increases from 0 to 1, the Si, Ge, and Sn matrices are softened by 55.1%, 40.4%, and 36.1%, respectively. We also find that the degree of softening caused by sodiation is much more substantial than by lithiation (39.7%, 29.1%, and 1.5%, respectively), which is likely attributed to the particular atomic arrangement of c-Na$_y$M alloys at Na:M = 1:1 ratio. As shown in Figure S2, the c-NaM phases are composed of tetrahedral M clusters surrounded by Na atoms. Such arrangements lack extended M networks to provide strong resistance to deformation, resulting in the lower B values. Conversely, lithiated c-Li$_y$M alloys at Li:M = 1:1 ratio still retain well-connected M sublattices, which are composed of three-folded M atomic layers in puckered conformation,[21,22,39] and are thereby more resistive to deformation (higher B values).

B.3. Na Diffusion Behavior. AIMD simulations were performed to predict the diffusivity of Na (D_{Na}) at room temperature in the a-NaM alloys; (Na/M = 1 was used as it is the fully sodiated phase for Si and Ge). For each alloy, the mean-square displacements (MSD) of chosen atoms were calculated by averaging three different samples at a given temperature (800, 1000, and 1200 K); MSD = $|R_i(t) - R_i(0)|^2$, where $R_i(t)$ is the position of atom i at time t. The Einstein relation $D = \langle \mathrm{MSD} \rangle / 6t$, with the MSD profiles was used to estimate D_{Na} values; the angle brackets indicate the ensemble average over an AIMD simulation time. We typically ran AIMD up to 10 ps, which appears to be sufficient to obtain well converged results. After disregarding the first 2 ps, we estimated the reported D_{Na} values from linear fits over a time interval of the following 8 ps and constructed an Arrhenius plot of $\ln(D_{Na})$ versus $1000/T$ based on D_{Na} at different temperatures for each alloy system (see Figure S3); here, the temperature was controlled using the Nose−Hoover thermostat. Predicted prefactor D_0, diffusion barrier E_a, and room-temperature D_{Na} values are summarized in Table 3.

Table 3. Predicted Activation Barriers (E_a), Prefactors (D_0), and Corresponding Diffusion Coefficients ($D_{Na} = D_0 \exp(E_a/k_BT)$) at T = 298 K for Na Atoms in a-NaM Alloys

	E_a (eV)	D_0 (cm^2/s)	D_{Na} (298 K) (cm^2/s)
Si	0.31	1.30×10^{-3}	8.13×10^{-9}
Ge	0.27	0.95×10^{-3}	2.87×10^{-8}
Sn	0.26	0.90×10^{-3}	3.66×10^{-8}

In comparison to single Na diffusion in c-M (as reported in section A.2), the E_a in a-NaM are predicted to be much smaller, especially for the case of Sn, where E_a is reduced from 1.08 eV in c-Sn to around 0.26 eV in a-NaSn. The predicted D_0 values are on the order of 10^{-3} s^{-1}, comparable to the prediction based on harmonic transition state theory.[40] Taking the D_0 and E_a values, we see that D_{Na} [$= D_0 \exp(-E_a/kT)$] in a-Na$_y$M of increasing y would rise by orders of magnitude from $\times 10^{-22}$, $\times 10^{-17}$, and $\times 10^{-12}$ cm^2/s (for single Na diffusion in c-Si, c-Ge, and c-Sn) to $\times 10^{-9}$, $\times 10^{-8}$, and $\times 10^{-8}$ cm^2/s in a-NaSi, a-NaGe, and a-NaSn, respectively. The drastic increase of Li diffusivity has also been demonstrated during lithiation,[41] which can be well explained by the fact that both lithiation and sodiation cause the host matrices to undergo softening and disintegration.

While both D_{Na} and D_{Li} are very sensitive to the host materials only at early stages of solidiation/lithiation, the former tend to be orders of magnitude smaller, especially near the onset of sodiation/lithiation (i.e., single Na or Li diffusion in c-M). Once the host matrices are moderately sodiated, D_{Na} in a-NaM alloys become comparable in value, as also seen in the lithiated cases.[24] Notice also that D_{Na} in a-NaM are predicted to be approximately 1 order of magnitude larger than D_{Li} in a-LiSi ($\approx 5.16 \times 10^{-10}$ cm^2/s),[41] although Na is larger and heavier than Li. One possible explanation may be that given the atomic arrangement (i.e., compact M fragments/clusters dispersed in Na), Na may undergo diffusion in a-NaM while experiencing less interactions with the host atoms. That is Na diffusion would be very similar to the case of self-diffusion, where the experimentally measured Na self-diffusivity at room temperature is relatively high ($\approx 10^{-8}$ cm^2/s),[42] similar to our predicted D_{Na} values in a-NaM.

In short, our results highlight that the sodiation process, involving Na incorporation and diffusion, is constantly evolving and becomes more facile with increasing Na content. This finding not only clarifies the relationship between D_{Na} (D_{Li}) and host materials at different stages of sodiation (lithiation) but also brings on a new perspective to reevaluate Si as an anode material for NIBs. That is, utilization of presodiated Si (instead of pure Si) in combination with controlled cycling voltage (i.e., Si is never fully desodiated) would be a viable approach to the favorable sodiation of Si, although its initial capacity will decrease to a certain extent; this might warrant further experimental investigations.

4. SUMMARY

Comparative analyses based on DFT-GGA calculations were carried out to examine the sodiation behaviors of group IV semiconductors (= Si, Ge, Sn). We first examined the incorporation and diffusion of an isolated Na atom in the crystalline host matrices (c-M), and then the formation energetics and structural/mechanical/diffusion properties of Na−M alloys with varying Na contents. While a Na atom is found to favorably exist at a tetrahedral interstitial site in the diamond structure of M, the Na-induced lattice disturbance is minimal in Sn but significant in Si (due to its relatively smaller interstitial space and higher stiffness). As such, Na incorporation is predicted to be the least and most favorable in Si and Sn, respectively, which tends to be predominantly attributed to the electronic effect rather than the strain effect. That is, although the relatively softer Sn lattice enables flexible expansion to incorporate the Na interstitial, the favorable Na−Sn bonding interaction contributes more substantially to the overall stabilization of the system upon Na accommodation. According to our Bader charge analysis, there is significant electron transfer from Na to the host matrices (0.67e, 0.71e, and 0.74e in Si, Ge, and Sn, respectively). We also find significant hybridization between the Na 3sp^3 and Si 3sp^3 states, indicating a high degree of covalency, while the covalent bonding

DOI: 10.1021/acs.jpcc.5b01099
J. Phys. Chem. C 2015, 119, 14843−14850

contribution dwindles as the host matrix changes from Si to Ge to Sn. Our calculations predict that a Na interstitial undergoes migration by overcoming relatively larger barriers (E_a) than required for Li diffusion: E_a for Na (Li) diffusion was calculated to be 1.08 (0.62), 0.78 (0.44), and 0.53 (0.39) eV in Si, Ge, and Sn, respectively. Based on our DFT calculations, it is clear that the formation and migration of interstitial Na (Li) in *c*-M are highly dependent on the flexibility of M lattice, as well as the relative sizes and interaction between Na (Li) and M. Overall, our results are consistent with the trend predicted at the onset of lithiation. Among the three host materials considered, Na incorporation (in the dilute concentration) is found to be the most facile in Sn and the least so in Si.

AIMD simulations were employed to determine the structure of *a*-Na−M in terms of Na content. The predicted mixing/formation enthalpies of the amorphous alloys demonstrate that Na alloying with M is energetically favorable while the most favorable compositions are predicted to occur around Na:M = 1:1 for M = Si and Ge, while 3.75:1 for Sn. The volume of the *a*-Na_yM alloys tends to increase nearly linearly with *y*, which is also the case for lithiated *a*-Li_yM; only the degree of expansion is more excessive during the sodiation process. The amounts of volume expansion for *a*-NaSi, *a*-NaGe, and *a*-$Na_{3.75}Sn$ are predicted to be about 230%, 200%, and 480%, respectively, as compared to corresponding volume expansions of 160%, 140%, and 260% for *a*-LiSi, *a*-LiGe, and *a*-$Li_{3.75}Sn$. As the Na content increases, the host lattice weakens and undergoes disintegration to form compact clusters. The structural changes cause softening of the Na−M alloys. According to our calculations, the bulk modulus (B) of crystalline Na_yM alloys is reduced by 55.1% (Si), 40.4% (Ge), and 36.1% (Sn) as *y* increases from 0 to 1. Interestingly, the degree of softening is noticeably greater compared to what was predicted for corresponding lithiated *c*-Li*M*, i.e., 39.7% (Si), 29.1% (Ge), and 1.5% (Sn). This is likely attributed to the specific atomic arrangement; that is, the formation of isolated *M* clusters leads to the loss of lattice connectivity in the NaM alloys, thereby lowering the B values. Lastly, the room-temperature diffusion coefficients of Na (D_{Na}) in sodiated Si, Ge, and Sn were estimated. Our results indicate that D_{Na} is highly sensitive to the host material only at early stages of sodiation. Once the host matrices are moderately sodiated, D_{Na} in *a*-NaM alloys become comparable in value. Owing to the formation of compact M clusters in highly sodiated phases (≈ *a*-NaM), D_{Na} are predicted to approach the experimentally measured self-diffusivity (around 10^{-8} cm^2/s at room temperature), approximately 1 order of magnitude larger than D_{Li} in *a*-LiSi despite the heavier and larger size of Na.

As highlighted by our results, the sodiation of Si, Ge, and Sn share many similarities with their corresponding lithiation processes; both are constantly evolving and become more facile with increasing alkali content. Sn, as a host material, demonstrates clear advantages over Ge and Si during the initial stages of sodiation; however, such distinctions among the three alloy systems tend to diminish quickly in their highly sodiated phases. This understanding in turn hints at the possibility of utilizing presodiated Si to overcome the sluggish sodiation at the cost of a slightly compromised initial capacity. Overall, these fundamental findings add to the understanding of the sodiation behavior of Si, Ge, and Sn as well as the properties of *a*-Na_yM alloys. Furthermore, the improved understanding from the comparative study of the sodiation versus lithiation processes can help develop next-generation anode materials for Na-ion batteries.

■ ASSOCIATED CONTENT

Supporting Information

AIMD snapshots of *a*-Na_yM (M = Si, Ge, and Sn; $0.33 \leq y \leq 3$), optimized atomic configurations of *c*-NaM, Arrhenius plots constructed for estimation of Na diffusion parameters, and additional calculation results including the restoring forces experienced by a Na atom upon displacement as well as the lattice constants of *c*-NaM and *c*-$Na_{15}M_4$. The Supporting Information is available free of charge on the ACS Publications website at DOI: 10.1021/acs.jpcc.5b01099.

■ AUTHOR INFORMATION

Corresponding Author

*Tel 1-512-471-4847, Fax 1-512-471-7060, e-mail gshwang@che.utexas.edu (G.S.H.).

Notes

The authors declare no competing financial interest.

■ ACKNOWLEDGMENTS

This work was supported by the Robert A. Welch foundation (F-1535). We thank the Texas Advanced Computing Center for use of their computing resources.

■ REFERENCES

(1) Nishi, Y. Lithium Ion Secondary Batteries; Past 10 Years and The Future. *J. Power Sources* **2001**, *100*, 101−106.
(2) Tarascon, J.-M.; Armand, M. Issues and Challenges Facing Rechargeable Lithium Batteries. *Nature* **2001**, *414*, 359−367.
(3) Ellis, B. L.; Nazar, L. F. Sodium and Sodium-Ion Energy Storage Batteries. *Curr. Opin. Solid State Mater. Sci.* **2012**, *16*, 168−177.
(4) Teng, F.-Z.; McDonough, W. F.; Rudnick, R. L.; Dalpe, C.; Tomascak, P. B.; Chappell, B. W.; Gao, S. Lithium Isotopic Composition and Concentration of the Upper Continental Crust. *Geochim. Cosmochim. Acta* **2004**, *68*, 4167−4178.
(5) Seyfried, W. E., Jr.; Janecky, D. R.; Mottl, M. J. Alteration of the Oceanic Crust: Implications for Geochemical Cycles of Lithium and Boron. *Geochim. Cosmochim. Acta* **1984**, *48*, 557−569.
(6) Yaksic, A.; Tilton, J. E. Using the Cumulative Availability Curve to Assess the Threat of Mineral Depletion: the Case of Lithium. *Resour. Policy* **2009**, *34*, 185−194.
(7) Kim, S.-W.; Seo, D.-H.; Ma, X.; Ceder, G.; Kang, K. Electrode Materials for Rechargeable Sodium-Ion Batteries: Potential Alternatives to Current Lithium-ion Batteries. *Adv. Energy Mater.* **2012**, *2*, 710−721.
(8) Stevens, D. A.; Dahn, J. R. The Mechanisms of Lithium and Sodium Insertion in Carbon Materials. *J. Electrochem. Soc.* **2001**, *148*, A803−A811.
(9) Chevrier, V. L.; Ceder, G. Challenges for Na-Ion Negative Electrodes. *J. Electrochem. Soc.* **2011**, *158*, A1011−A1014.
(10) Ge, P. Electrochemical Intercalation of Sodium in Graphite. *Solid State Ionics.* **1988**, *28−30*, 1172−1175.
(11) Baggetto, L.; Ganesh, P.; Sun, C.-N.; Meisner, R. A.; Zawodzinski, T. A.; Veith, G. M. Intrinsic Thermodynamic and Kinetic Properties of Sb Electrodes for Li-Ion and Na-Ion Batteries: Experiment and Theory. *J. Mater. Chem. A* **2013**, *1*, 7985−7994.
(12) Darwiche, A.; Marino, C.; Sougrati, M. T.; Fraisse, B.; Stievano, L.; Monconduit, L. Better Cycling Performances of Bulk Sb in Na-Ion Batteries Compared to Li-Ion Systems: An Unexpected Electrochemical Mechanism. *J. Am. Chem. Soc.* **2012**, *134*, 20805−20811.
(13) Yamamoto, T.; Nohira, T.; Hagiwara, R.; Fukunaga, A.; Sakai, S.; Nitta, K.; Inazawa, S. Charge-Discharge Behavior of Tin Negative Electrode for A Sodium Secondary Battery Using Intermediate Temperature Ionic Liquid Sodium Bis(fluorosulfonyl)amide-Potassium Bis(fluorosulfonyl)amide. *J. Power Sources* **2012**, *217*, 479−484.

DOI: 10.1021/acs.jpcc.5b01099
J. Phys. Chem. C 2015, 119, 14843−14850

(14) Ellis, L. D.; Ferguson, P. P.; Obrovac, M. N. Sodium Insertion Into Tin Cobalt Carbon Active/Inactive Nanocomposite. *J. Electrochem. Soc.* **2013**, *160*, A869−A872.
(15) Park, C.-M.; Kim, J.-H.; Kim, H.; Sohn, H.-J. Li-Alloy Based Anode Materials for Li Secondary Batteries. *Chem. Soc. Rev.* **2010**, *39*, 3115−3141.
(16) Zhang, W. J. A Review of the Electrochemical Performance of Alloy Anodes for Lithium-Ion Batteries. *J. Power Sources* **2011**, *196*, 13−24.
(17) Kasavajjula, U.; Wang, C.; Appleby, A. J. Nano- and Bulk-Silicon-Based Insertion Anodes for Lithium-Ion Secondary Cells. *J. Power Sources* **2007**, *163*, 1003−1039.
(18) Chen, C. K.; Zhang, X. F.; Cui, Y. High Capacity Li Ion Battery Anodes Using Ge Nanowires. *Nano Lett.* **2008**, *8*, 307−309.
(19) Winter, M.; Besenhard, J. O. Electrochemical Lithiation of Tin and Tin-Based Intermetallics and Composites. *Electrochim. Acta* **1999**, *45*, 31−50.
(20) Palomares, V.; Serras, P.; Villaluenga, I.; Hueso, K. B.; Carretero-González, J.; Rojo, T. Na-Ion Batteries, Recent Advances and Present Challenges to Become Low Cost Energy Storage Systems. *Energy Environ. Sci.* **2012**, *5*, 5884−5901.
(21) Shenoy, V. B.; Johari, P.; Qi, Y. Elastic Softening of Amorphous and Crystalline Li-Si Phases with Increasing Li Concentration: A First-Principles Study. *J. Power Sources* **2010**, *195*, 6825−6830.
(22) Stournara, M. E.; Guduru, P. R.; Shenoy, V. B. Elastic Behavior of Crystalline Li-Sn Phases with Increasing Li Concentration. *J. Power Sources* **2012**, *208*, 165−169.
(23) Chan, M. K. Y.; Long, B. R.; Gewirth, A. A.; Greeley, J. P. The First-Cycle Electrochemical Lithiation of Crystalline Ge: Dopant and Orientation Dependence and Comparison with Si. *J. Phys. Chem. Lett.* **2011**, *2*, 3092−3095.
(24) Chou, C.-Y.; Kim, H.; Hwang, G. S. A Comparative First-Principles Study of the Structure, Energetics, and Properties of Li-M (M = Si, Ge, Sn) Alloys. *J. Phys. Chem. C* **2011**, *115*, 20018−20026.
(25) Lide, D. R., Ed.; *CRC Handbook of Chemistry and Physics*, 80th ed.; CRC Press: Boca Raton, FL, 1999; p 14.
(26) Blöchl, P. E. Pojector Augmented-Wave Method. *Phys. Rev. B* **1994**, *50*, 17953−17979.
(27) Kresse, G.; Hafner, J. Ab Initio Molecular Dynamics of Liquid Metals. *Phys. Rev. B* **1993**, *47*, 558−561.
(28) Kresse, G.; Furthmuller, J. Efficiency of Ab-Initio Total Energy Calculations for Metals and Semiconductors Using a Plane-Wave Basis Set. *Comput. Mater. Sci.* **1996**, *6*, 15−50.
(29) Kresse, G.; Furthmuller. Efficient Iterative Schemes for Ab Initio Total-Energy Calculations Using a Plane-Wave Basis Set. *J. Phys. Rev. B* **1996**, *54*, 11169−11186.
(30) Monkhorst, H. J.; Pack, J. D. Special Points for Brillouin-Zone Integrations. *Phys. Rev. B* **1976**, *13*, 5188−5192.
(31) Henkelman, G.; Uberuaga, B. P.; Jonsson, H. A Climbing Image Nudged Elastic Band Method for Finding Saddle Points and Minimum Energy Paths. *J. Chem. Phys.* **2000**, *113*, 9901−9904.
(32) Kim, H.; Chou, C.-Y.; Ekerdt, J. G.; Hwang, G. S. Structure and Properties of Li-Si Alloys: A First-Principles Study. *J. Phys. Chem. C* **2011**, *115*, 2514−2521.
(33) Baggetto, L.; Ganesh, P.; Meisner, R. P.; Unocic, R. R.; Jumas, J.-C.; Bridges, C. A.; Veith, G. M. Characterization of Sodium Ion Electrochemical Reaction with Tin Anodes: Experiment and Theory. *J. Power Sources* **2013**, *234*, 48−59.
(34) Baggetto, L.; Keum, J. K.; Browning, J. F.; Veith, G. M. Germanium as Negative Electrode Material for Sodium-Ion Batteries. *Electrochem. Commun.* **2013**, *34*, 41−44.
(35) Farbod, B.; Cui, K.; Kalisvaart, W. P.; Kupsta, M.; Zahiri, B.; Kohandehghan, A.; Lotfabad, E. M.; Li, Z.; Luber, E. J.; Mitlin, D. Anodes for Sodium Ion Batteries Based on Tin-Germanium-Antimony Alloys. *ACS Nano* **2014**, *8*, 4415−4429.
(36) Liu, Y. Virus Enabled 3D Nano-Array Electrodes for Intergrated Li/Na-Ion Microbatteries. Thesis, University of Maryland, 2013.
(37) Murnaghan, F. D. The Compressibility of Media Under Extreme Pressures. *Proc. Natl. Acad. Sci. U. S. A.* **1944**, *30*, 244−247.
(38) Mortazavi, M.; Deng, J.; Shenoy, V. B.; Medhekar, N. V. Elastic Softening of Alloy Negative Electrodes for Na-Ion Batteries. *J. Power Sources* **2013**, *225*, 207−214.
(39) Genser, O.; Hafner, J. First-Principles Studies of the Stability of Zintl Ions In Alkali-Tin Alloys: I. Crystalline Intermetallic Compounds. *J. Phys.: Condens. Matter.* **2001**, *13*, 959−980.
(40) Wang, X. R.; Xiao, X.; Zhang, Z. Apparent Anomalous Prefactor Enhancement for Surface Diffusion Due to Surface Defects. *Surf. Sci.* **2002**, *512*, L361−L366.
(41) Chou, C.-Y.; Hwang, G. S. On the Origin of the Significant Difference in Lithiation Behavior Between Silicon and Germanium. *J. Power Sources* **2014**, *263*, 252−258.
(42) Nowick, A. S. *Diffusion in Solids: Recent Developments*; Elsevier: Amsterdam, 2012; p 133.

DOI: 10.1021/acs.jpcc.5b01099
J. Phys. Chem. C 2015, 119, 14843−14850